Chinese Chemical Letters 34 (2023) 107547

Contents lists available at ScienceDirect

Chinese Chemical Letters

journal homepage: www.elsevier.com/locate/cclet

Switching the coordination geometry to enhance erbium(III) single-molecule magnets

Qian-Cheng Luo[a], Ning Ge[a], Yuan-Qi Zhai[a], Tengbo Wang[b], Lin Sun[c], Qi Sun[d], Fanni Li[e], Zhendong Fu[f,*], Yan-Zhen Zheng[a,*]

[a] Frontier Institute of Science and Technology, School of Chemistry and School of Physics, Xi'an Jiaotong University, Xi'an 710054, China
[b] The School of Automation Science and Technology, Xi'an Jiaotong University, Xi'an 712000, China
[c] Institute of Molecular and Crystal Engineering, College of Chemistry and Chemical Engineering, Henan University, Kaifeng 475004, China
[d] Department of General Surgery, The First Affiliated Hospital of Xi'an Jiaotong University, Xi'an 710061, China
[e] Department of Talent Highland, The First Affiliated Hospital of Xi'an Jiaotong University, Xi'an 710061, China
[f] Neutron Platform, Songshan Lake Materials Laboratory, Dongguan 523808, China

ARTICLE INFO

Article history:
Received 24 April 2022
Revised 6 May 2022
Accepted 18 May 2022
Available online 23 May 2022

Keywords:
Single-molecule magnets
Erbium
Lanthanide complexes
Magnetic anisotropy
Slow magnetic relaxation

ABSTRACT

Two erbium(III) complexes $[ErCl(OAr^{Ad})_3][Na(THF)_6]$ (**1**) and $Er(OAr^{Ad})_3$ (**2**) are successfully prepared by using one variety of "hard" base ligand with large steric hindrance. The coordination geometry around the Er(III) site changes from distorted tetrahedral to flat trigonal pyramid geometry in different solvent environment due to the removal of the coordinated chloride. Such an alternation significantly enhances the single-molecule magnet (SMM) behavior and makes the field-induced effective energy barrier (U_{eff}) arrive at 43(1) cm^{-1} for the latter. Together with theoretical calculations, this study shows that strong equatorial ligand field and high local symmetry are critical to suppress the quantum tunneling of the magnetization (QTM) and achieve high-performance erbium(III) based SMMs.

Single-molecule magnets (SMMs), a type of magnetic nanomaterials self-assembled by coordination chemistry, is appealing due to their inherent characteristics of possessing magnetic bistability and slow magnetic relaxation processes. The feature of storing bytes information relaying on single molecule improves information storage density, making it possible for the applications of spintronic devices and quantum information processing (QIP) [1–3]. Since the mononuclear complex $[TbPc_2]^-$ (Pc = dianion of phthalocyanine), whose effective energy barrier (U_{eff}) is 230 cm^{-1}, was reported by Ishikawa *et al.* [4], lanthanide cations, such as Tb(III), Dy(III), Ho(III) and Er(III), have been attached importance to construct high performance SMMs in the light of their high magnetic anisotropy and strong spin-orbit coupling effects [5–9]. For almost a decade, enormous progress for enhancing U_{eff} and magnetic blocking temperature (T_B) has been made for lanthanide-based complexes, which are almost Dy(III) compounds [10,11]. Especially lately, a record-breaking mixed-valence dilanthanide complex $(Cp^{iPr5})_2Dy_2I_3$ with U_{eff} of 1631 cm^{-1} and T_B of 72 K was reported by Gould *et al.* [12].

Despite the fact that the performance of Er(III) SMMs is relatively poor by contrast with Dy(III)-based counterparts, it is better than SMMs with other prolate Ln(III) ions. A series of reported mononuclear Er(III) SMMs are listed in Tables S12 and S13 (Supporting information), where the highest U_{eff} of 300 cm^{-1} can be observed in $[(C_5H_5BMe)Er(COT)]$ (COT = cyclooctatetraenyl) [13], and the maximum T_B does not exceed 10 K in several (cyclooctatetraenyl) erbium(III) complexes [14–16]. It is evident that the COT ligand can stabilize magnetic ground state of Er(III) and makes those complexes with sandwich structure exhibit excellent SMM properties. Apart from those organometallic Er(III) compounds, SMMs with monodentate coordination have also been exploited and reported all the time (Table S13). Zhang *et al.* prepared an equatorially nitrogen-coordinated complex with C_{3v} local geometry $Er[N(SiMe_3)_2]_3$ which possesses an energy barrier of 85 cm^{-1} in the absence of a static field [17]. Similarly, two three-coordinate Er(III) compounds with oxygen and carbon donors were reported by Zhang *et al.* [18], namely $Er(dbpc)_3$ (dbpc = tris(2,6-di-*tert*-butyl-*p*-cresolate)) and $Er(btmsm)_3$ (btmsm = tris(bis(trimethylsilyl)methyl)), exhibiting lower U_{eff} values of 39 and 80 cm^{-1}, because of the conjugation effects and weak lone pairs for the former and soft carbon donor effect for the latter, respectively.

* Corresponding authors.
E-mail addresses: zdfu@pku.edu.cn (Z. Fu), yanzhen@nankai.edu.cn (Y.-Z. Zheng).

https://doi.org/10.1016/j.cclet.2022.05.061
1001-8417/

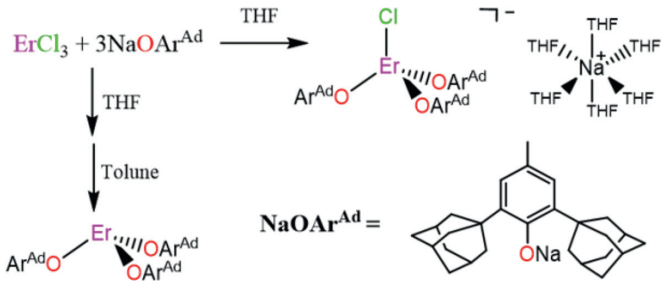

Scheme 1. Synthesis of complexes **1** and **2**.

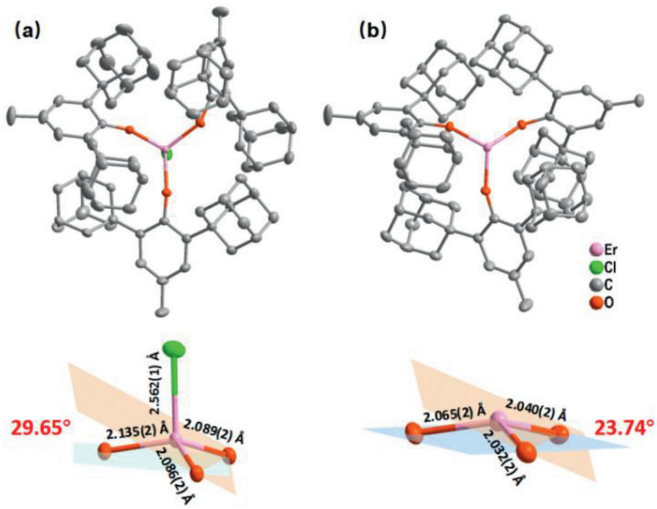

Fig. 1. (Top) Crystal structures of (a) **1** and (b) **2**. color codes: Er, pink; O, red; C, gray; Cl, green. All hydrogen atoms have been omitted for clarity. (Bottom) The diagrammatic sketch of ErO_3Cl and ErO_3 geometry for **1** and **2**, respectively. The angles represent average dihedral angles between coordinate plane and center-donor plane.

Stark energy level splitting is sensitive to the coordination sphere and appropriate crystal field environment plays a critical role to construct high-performance SMMs: Long and his coworkers point out that equatorial coordination environments is more conducive for those prolate 4f ions, for instance, Yb(III) and Er(III), because it can reduce and avoid charge contact between axially located electron density of Ln(III) ions and coordination atoms [19]. Furthermore, the existence of quantum tunneling of the magnetization (QTM) leads to under barrier relaxation pathways and poor SMM properties, and high local symmetry around Ln(III) ions is capable of suppressing such fast relaxation process which has been confirmed by both theoretical and experimental results [20–27]. Herein, considering prolate electron density of Er(III), we utilized one variety of "hard" base ligand with large steric hindrance (-OAr^{Ad}) and successfully isolated two complexes **1** ($[ErCl(OAr^{Ad})_3][Na(THF)_6]$) and **2** ($Er(OAr^{Ad})_3$). Remarkably, ac susceptibility measurements reveal that out-of-phase (χ") signals can be observed in complex **1** at dc magnetic field of 800 Oe and **2** at zero dc field, and field-induced Orbach barrier height of **2** arrives at 43(1) cm^{-1} (61(2) K).

The sterically demanding aryloxide ligand, $^{Ad}ArOH$ (^{Ad}ArO = O-C_6H_2-2,6-Ad-4-Me), was synthesized following a procedure from Watanabe *et al.* [28]. The corresponding deprotonated salt, $NaOAr^{Ad}$, was prepared in 94% yield by addition of NaH to the phenol in THF suspension. The mixed aryloxide-chloride $[ErCl(OAr^{Ad})_3][Na(THF)_6]$ (**1**) was prepared by metathesis of anhydrous $ErCl_3$ with 3 equiv. of $NaOAr^{Ad}$ in THF, giving a pink crystal in 60% yield (Scheme 1). Treating **1** with toluene resulted in the formation of chloride free $Er(OAr^{Ad})_3$ (**2**), which could be isolated as a pinkish crystal in 42% (Scheme 1).

X-Ray single-crystal diffraction analysis reveals that **1** and **2** crystallize in the monoclinic $P2_1/c$ and triclinic $P\bar{1}$ space groups (Table S1), respectively. Compound **1** is composed of four-coordinate Er(III) anions with distorted tetrahedral configuration ($[ErCl(OAr^{Ad})_3]^-$) and charge-balancing cations $[Na(THF)_6]^+$, while electrically neutral complex **2** is characteristic of a flat trigonal pyramid, in which Er(III) ion is coordinated with three -OAr^{Ad} ligands with large steric hindrance (Fig. 1). The Er-Cl bond length in **1** is 2.562(1) Å and the average distance of Er-O bonds is 2.103 Å. In contrast to **1**, the elimination of Cl^- ion leads to shorter average distance of Er-O bonds (2.046 Å) and smaller structural distortion relative to planar triangle geometry in **2** (Fig. 1 and Table S2 in Supporting information). These Er-O distances are close to several reported Er(III) SMMs containing merely monodentate oxygen donors but significantly shorter than $[L_2Er(H_2O)_5][I]_3{\cdot}L_2{\cdot}(H_2O)$ (L = ^{t}BuPO(NH^{i}Pr)$_2$) and $[Er(depma)_2(H_2O)_6]Cl_3{\cdot}6H_2O$ (depma = 9-diethylphosphonomethylanthracene) (Table S13). Meanwhile, three O-Er-O angles in both complexes range from 105.84(9)° to 120.27(9)° for **1** and 111.99(9)° to 119.93(9)° for **2**. In a packing diagrams, the shortest intermolecular Er···Er distances are 12.954(1) and 14.747(1) Å (Figs. S1 and S2 in Supporting information), suggesting that both complexes are well isolated and intermolecular magnetic interactions are negligible.

The temperature dependent dc magnetic susceptibility measurements were carried out towards the powder samples of **1** and **2** at the temperature range of 2–300 K under an applied field of 1000 Oe (Figs. S3 and S4 in Supporting information). At the room temperature, the experimental $\chi_M T$ products of both compounds are 11.06 and 11.36 cm^3 K/mol, respectively, which are agreement with theoretical value of 11.48 cm^3 K/mol for free Er(III) ion ($S = 3/2$, $L = 6$, $g = 6/5$). The $\chi_M T$ value undergoes a gradual decrease when lowering the temperature and arrives at the minimum of 9.75 and 8.69 cm^3 K/mol at 2 K for **1** and **2** respectively, which can be attributed to the thermal depopulation of the Stark levels from Er(III) ions [29]. A relatively more drastic drop of **2** than **1** at low temperature below 10 K can also be observed, indicating its characteristic of slower magnetic relaxation. The field dependent dc magnetization data of them were also measured from 0 to 5 T at 2 K (Figs. S5 and S6 in Supporting information). The magnetization increases linearly at low magnetic fields until around 0.5 T and reaches similar saturation values of 4.78 and 4.65 μ_B for **1** and **2**, respectively.

Dynamic magnetic properties of **1** and **2** were investigated in the frequency range of 1–1218 Hz through ac magnetic susceptibility measurements. Under zero dc field, significant out-of-phase (χ") signal can be observed only in complex **2** and the peak of χ" shifts from 2 K to 10.19 K (Figs. S12 and S13 in Supporting information), demonstrating its slow magnetic relaxation behavior and SMM characteristic while strong QTM exists in **1** (Fig. S7 in Supporting information) [30]. To confirm the optimum field and study their dynamic magnetic behavior under dc field, ac measurements were performed under the magnetic field range of 0–2000 Oe at 2 K (for **1**) and 5 K (for **2**). Finally, the field of 800 and 1000 Oe were adopted for **1** and **2** in the light of measured strongest out-of-phase signals (Figs. S8 and S14 in Supporting information). Under this condition, frequency dependence of χ" peaks can be observed from 3.57 K to 8.25 K for **1** and 4.92 K to 12.50 K for **2** in measured frequency range (Figs. S10 and S16 in Supporting information). Then relaxation times (τ) were extracted by the generalized Debye model and all Cole-Cole plots indicates the presence of one relaxation process (Figs. S11, S17 and S18 in Supporting information). Further investigation of magnetic relaxation processes can

Table 1
Best-fit parameters of temperature-dependent relaxation times for **1** and **2**.

Parameter	τ_0 (s)	U_{eff} (cm^{-1})	C (K^{-n} s^{-1})	n	τ_{QTM} (s)
1 (800 Oe)	–	–	$2.5(6)\times10^{-4}$	7.9(1)	–
2 (0 Oe)	–	–	0.147(1)	4.5(1)	$8(2)\times10^{-4}$
2 (1000 Oe)	$1.2(5)\times10^{-6}$	43(1)	0.07(1)	4(1)	–

be achieved by the temperature dependence of τ and analysed by the plots of τ^{-1} *vs.* T (Figs. S19–S22 in Supporting information). For **1** under dc field of 800 Oe, its relaxation behavior can be well-modelled only considering individual Raman process (Eq. 1). An additional term to account for QTM process was required to fit the relaxation behavior of **2** under zero dc field due to slow variation of τ^{-1} value in the low temperature region (Eq. 2). Moreover, for **2** under dc field of 1000 Oe, only the combination of Orbach and Raman mechanisms can well describe the relationship between τ^{-1} and T (Eq. 3). The best fit parameters are summarized in Table 1. It is obvious that the coordination of Cl^- ion induces strong QTM process and the elimination of this coordinated chloride suppresses the fast relaxation processes, leading to field-induced effective energy barrier value (U_{eff}) of **2** arrives at 43(1) cm^{-1} (61(2) K).

$$\tau^{-1} = CT^n \tag{1}$$

$$\tau^{-1} = CT^n + \tau_{QTM}^{-1} \tag{2}$$

$$\tau^{-1} = \tau_0^{-1}\exp\left(-U_{eff}/k_BT\right) + CT^n \tag{3}$$

Complete-active-space self-consistent filed spin-orbit (CASSCF-SO) calculations were performed using OPEN MOLCAS package [31] to further understand magnetic relaxation mechanisms of **1** and **2**. Evidently, calculated g-tensors of the ground Kramers' doublet (KD) for both complexes are $g_x = 0.03$, $g_y = 0.04$, $g_z = 17.82$ for **1** and $g_x = g_y = 0.02$, $g_z = 17.80$ for **2** (Tables S3 and S4 in Supporting information), indicating they possess large magnetic anisotropy. Meanwhile, the predominant wavefunction composition (89.5% $|\pm 15/2>$ for **1** and 98.5% $|\pm15/2>$ for **2**) and the direction of principal magnetic axes (Figs. S23 and S24 in Supporting information) for the ground KD also verify this. We find that the orientation of easy axis is not exactly along Er-Cl bond for the former or perpendicular to the plane composed of three coordinated O atoms for the latter, existing a certain deviation, which could be caused by the structural distortions compared with the strict local symmetry of T_d or C_{3v} from the perspective of molecular geometric configuration [32]. For **1**, the admixture of wavefunction emerges at the first excited KD (63.8% $|\pm13/2> + 18.7\%$ $|\pm11/2>$) and relatively significant transition magnetic moment between this KD arrives at $\sim10^{-1}$ μ_B, therefore a fast QTM process will occur at this KD theoretically, making the calculated U_{eff} is around 61 cm^{-1} (88 K) (Table S9 and Fig. S27a in Supporting information). Nevertheless, non-ignorable transition probability of 1.20×10^{-2} μ_B between the ground KD can be also observed, hinting that a non-vanishing QTM may exist. In reality, two-phonon Raman process also participate in the magnetic relaxation in the temperature range of ac measurement at the same time. Computed LoProp charge of donor Cl using the CASSCF wavefunctions is up to −0.8303, and the poor SMM property of **1** can be attributed to the energy destabilization of the prolate Er(III) ion induced by rather strong repulsion with axial highly charged Cl^- ion (Fig. S26 in Supporting information) [19,33]. Accordingly, with axial ligand eliminated, the coordination environment of **2** containing merely three O atoms is more suitable for Er(III) ion: The energy gap between the ground KD and the first low-lying state is greatly improved to 155 cm^{-1} (223 K) (Table S4), and the absolute value of axial crystal-field parameters (CFPs) of **2** ($B_2^0 = -3.32$ cm^{-1}, $B_4^0 = 2.37\times10^{-3}$ cm^{-1} and $B_6^0 = -2.81\times10^{-5}$ cm^{-1}) are significantly larger than **1** ($B_2^0 = -1.94$ cm^{-1}, $B_4^0 = 1.27\times10^{-3}$ cm^{-1} and $B_6^0 = -6.78\times10^{-6}$ cm^{-1}) and smaller magnitude of non-axial CFP (B_k^q, $q \neq 0$) can be observed in **2** (Tables S6 and S7), indicating stronger axial anisotropy in **2**. Besides, the admixture of wavefunction in **2** does not emerge until the fourth excited KD (78.5% $|\pm7/2>$), and the principal magnetization axis of this doublet is also largely tilted from the ground KD. Despite this, transition probability of 1.07×10^{-1} μ_B between the second excited KD indicates the occurrence of QTM process in this KD and computed energy barrier of 224 cm^{-1} (322 K) (Table S10 and Fig. S27b in Supporting information). Similar to complex **1**, although calculated U_{eff} value is larger than the experimental value, it is indeed qualitatively reasonable in terms of the order if not considering other existing effects, such as off-resonance phonon modes and hyperfine interactions [34,35].

Then, their relaxation times for QTM process at the ground KD were evaluated theoretically through Eqs. 4 and 5 proposed by Yin *et al.* [36]. Here, β is the Bohr magneton, h is Planck constant and the g_x, g_y and g_z are components of g tensor for the ground KD in x, y and z directions. The magnitude of the magnetic fields induced by dipolar and hyperfine interactions (H_{ave}) is estimated to be 20 mT because *ab initio* calculations can not provide this parameter from x to z directions directly and this selected value which can predict τ_{QTM} well was utilized in previously several reported systems [37,38]. The calculated τ_{QTM} of **1** is 4.63×10^{-5} s while this relaxation time for **2** (2.29×10^{-4} s) is almost five times than **1**, indicating faster QTM process occurs between the ground KD in **1** and it can explain why its slow magnetic relaxation behavior lacks under zero dc field. And computed τ_{QTM} for **2** is slightly smaller than the experimentally observed value at 2 K (8.57×10^{-4} s).

$$\tau_{QTM}^{-1} = \frac{\beta H_{ave}}{h}\cdot\frac{g_{xy}^2}{2\left(g_{xy}^2+g_z^2\right)^{1/2}} \tag{4}$$

$$g_{xy}^2 = \left(g_x^2 + g_y^2\right) \tag{5}$$

In spite of enhanced SMM performance in **2** realized by switching the coordination geometry from **1**, it is still poorer than its analogues, namely $Er[N(SiMe_3)_2]_3$, $Er(btmsm)_3$ and $Er(dbpc)_3$ (Table S13 in Supporting information). In our case, "hard" oxygen donor was utilized and the shifting is the lowest between Er(III) and the ligand coordination plane, however, we can observe that strong QTM process at absence of external field and lower field-induced Orbach energy barrier under dc magnetic field. For the former, the local symmetry around Er(III) ion in **2** is deviate more from C_{3v} than above-mentioned complexes in terms of bond lengths and angles which exacerbates its transverse magnetic anisotropy and fast relaxation under low temperature (Table S2). Additionally, similar to $Er(dbpc)_3$, the electron density of O donors with contracted lone pairs is delocalized on the aromatic ring, leading to the decrease of effective charge and lower U_{eff} value [18]. By contrast, as Yamashita *et al.* analyzed using the localized orbital locator (LOL), the lone pairs on coordinated C atoms in $Er(btmsm)_3$ diffuse towards central Er(III) and increase the effective charge, making it possess comparable U_{eff} value to $Er[N(SiMe_3)_2]_3$. Under such circumstances, further enhancement of magnetic relaxation properties can be achieved by improving local symmetry when using aryloxide ligands.

To further weaken transverse anisotropy of low-lying doublets and investigate the influence of local symmetry around Er(III) ion, model complex (**3**) with D_{3h} local symmetry was constructed in the light of the structure of **2** (Fig. S27c in Supporting information) and calculation at the same level was also carried out. The Er-O bonds in **3** were fixed as the average value of those in **2** (2.046 Å) and each angle of O-Er-O is perfectly 120°. As expected,

eight KDs span an energy barrier of 687 cm^{-1} (988 K) (Table S5 in Supporting information) and CFPs of complex **3** calculated by the SINGLE_ANISO program demonstrate its improved axiality with axial CFPs of $B_2^0 = -3.76$ cm^{-1} and $B_4^0 = 3.29 \times 10^{-3}$ cm^{-1}, despite nearly consistent parameter $B_6^0 = -2.38 \times 10^{-5}$ cm^{-1} with **2** (Table S8 in Supporting information). The calculated τ_{QTM} is up to 2.80×10^{-2} s and transition probability of 4.98×10^{-4} μ_B between the ground KD is small enough to be neglected (Table S11 in Supporting information). Above results demonstrate that improved local symmetry enlarges crystal field splitting of Er(III) ion and effectively suppresses QTM process under zero field condition. Significant QTM can be observed at the fourth excited KD (7.77×10^{-1} μ_B) and leads to theoretical U_{eff} value arrives at 416 cm^{-1} (598 K) (Fig. S27d in Supporting information), almost twice as much as **2**. This indicates that the crystal field environment with high local symmetry constructed by only coplanar equatorial coordinated atoms is conducive to greatly improve effective energy barrier of prolate Er(III) SMMs and it can be realized through modifying ligands by chemical means.

To summarize, we successfully isolated two Er(III) complexes by utilizing substituted phenols with large steric hindrance (-OAr^{Ad}) and they possess different geometry configurations in THF and toluene, respectively. Magnetic measurements reveal SMM behavior of both compounds and field-induced Orbach barrier height of complex **2** is 43(1) cm^{-1} (61(2) K). *Ab initio* calculations towards model complex **3** suggest that the removal of axial electrostatic repulsion and coplanar equatorial coordination pattern with high local symmetry are beneficial to further suppress QTM process and increase the U_{eff} value. Future work would include constructing more ideal crystal field environment to meet Er(III) ion with prolate electron density and improve the slow relaxation properties of complexes.

Declaration of competing interest

The authors declare that they have no known competing financial interests or personal relationships that could have appeared to influence the work reported in this paper.

Acknowledgments

This work was supported by National Natural Science Foundation of China (Nos. 21971203, 82073271 and 81803026), Key Scientific and Technological Innovation Team of Shaanxi Province (No. 2020TD-001) and the Fundamental Research Funds for Central Universities.

Supplementary materials

Supplementary material associated with this article can be found, in the online version, at doi:10.1016/j.cclet.2022.05.061.

References

[1] L. Bogani, W. Wernsdorfer, Nat. Mater. 7 (2008) 179–186.
[2] M.R. Wasielewski, M.D.E. Forbes, N.L. Frank, et al., Nat. Rev. Chem. 4 (2020) 490–504.
[3] S.L. Bayliss, D.W. Laorenza, P.J. Mintun, et al., Science 370 (2020) 1309–1312.
[4] N. Ishikawa, M. Sugita, T. Ishikawa, S.Y. Koshihara, Y. Kaizu, J. Am. Chem. Soc. 125 (2003) 8694–8695.
[5] V.S. Parmar, D.P. Mills, R.E.P. Winpenny, Chem. Eur. J. 27 (2021) 7625–7645.
[6] X. Liu, X. Feng, K.R. Meihaus, et al., Angew. Chem. Int. Ed. 59 (2020) 10610–10618.
[7] K. Liu, X.J. Zhang, X.X. Meng, et al., Chem. Soc. Rev. 45 (2016) 2423–2439.
[8] X.X. Meng, M.M. Wang, X.S. Gou, et al., Inorg. Chem. Front. 8 (2021) 2349–2355.
[9] S.W. Zhang, W. Shi, P. Cheng, Coord. Chem. Rev. 352 (2017) 108–150.
[10] F.S. Guo, B.M. Day, Y.C. Chen, et al., Science 362 (2018) 1400–1403.
[11] Y.S. Ding, N.F. Chilton, R.E.P. Winpenny, Y.Z. Zheng, Angew. Chem. Int. Ed. 55 (2016) 16071–16074.
[12] C.A. Gould, K.R. Mcclain, D. Reta, et al., Science 375 (2022) 198–202.
[13] Y.S. Meng, C.H. Wang, Y.Q. Zhang, et al., Inorg. Chem. Front. 3 (2016) 828–835.
[14] L. Münzfeld, C. Schoo, S. Bestgen, et al., Nat. Commun. 10 (2019) 3135.
[15] L. Ungur, J.J. Le Roy, I. Korobkov, M. Murugesu, L.F. Chibotaru, Angew. Chem. Int. Ed. 53 (2014) 4413–4417.
[16] K.R. Meihaus, J.R. Long, J. Am. Chem. Soc. 135 (2013) 17952–17957.
[17] P. Zhang, L. Zhang, C. Wang, et al., J. Am. Chem. Soc. 136 (2014) 4484–4487.
[18] H.T. Zhang, R. Nakanishi, K. Katoh, et al., Dalton Trans. 47 (2018) 302–305.
[19] J.D. Rinehart, J.R. Long, Chem. Sci. 2 (2011) 2078–2085.
[20] S.K. Gupta, T. Rajeshkumar, G. Rajaraman, R. Murugavel, Chem. Sci. 7 (2016) 5181–5191.
[21] M.A. Sørensen, U.B. Hansen, M. Perfetti, et al., Nat. Commun. 9 (2018) 1292.
[22] J.L. Liu, Y.C. Chen, Y.Z. Zheng, et al., Chem. Sci. 4 (2013) 3310–3316.
[23] Z.H. Li, Y.Q. Zhai, W.P. Chen, Y.S. Ding, Y.Z. Zheng, Chem. Eur. J. 25 (2019) 16219–16224.
[24] X.L. Ding, Y.Q. Zhai, T. Han, et al., Chem. Eur. J. 27 (2021) 2623–2627.
[25] J. Wu, O. Cador, X.L. Li, et al., Inorg. Chem. 56 (2017) 11211–11219.
[26] M.A. AlDamen, J.M. Clemente-Juan, E. Coronado, C. Martí-Gastaldo, A. Gaita-Ariño, J. Am. Chem. Soc. 130 (2008) 8874–8875.
[27] C.R. Ganivet, B. Ballesteros, G. de la Torre, et al., Chem. Eur. J. 19 (2013) 1457–1465.
[28] T. Watanabe, Y. Ishida, T. Matsuo, H. Kawaguchi, Dalton Trans. 39 (2010) 484–491.
[29] A.J. Brown, D. Pinkowicz, M.R. Saber, K.R. Dunbar, Angew. Chem. Int. Ed. 54 (2015) 5864–5868.
[30] J. Long, B.G. Shestakov, D. Liu, et al., Chem. Commun. 53 (2017) 4706–4709.
[31] I.F. Galván, M. Vacher, A. Alavi, et al., J. Chem. Theory Comput. 15 (2019) 5925–5964.
[32] S.K. Singh, B. Pandey, G. Velmurugan, G. Rajaraman, Dalton Trans. 46 (2017) 11913–11924.
[33] T.A. Bazhenova, V.A. Kopotkov, D.V. Korchagin, et al., Molecules 26 (2021) 6908.
[34] A. Lunghi, F. Totti, R. Sessoli, S. Sanvito, Nat. Commun. 8 (2016) 14620.
[35] F. Lu, M.M. Ding, J.X. Li, B.L. Wang, Y.Q. Zhang, Dalton Trans. 49 (2020) 14576–14583.
[36] B. Yin, C.C. Li, Phys. Chem. Chem. Phys. 22 (2020) 9923–9933.
[37] S. Zhang, J. Tang, J. Zhang, et al., Inorg. Chem. 60 (2021) 816–830.
[38] Y. Dong, L. Zhu, B. Yin, X. Zhu, D. Li, Dalton Trans. 50 (2021) 17328–17337.